AGU PUBLICATIONS

JGR

Journal of Geophysical Research: Oceans

RESEARCH ARTICLE

10.1002/2016JC011886

Assessment of net community production and calcification of a coral reef using a boundary layer approach

Yuichiro Takeshita[1,2], Wade McGillis[3], Ellen M. Briggs[1], Amanda L. Carter[1], Emily M. Donham[4,5], Todd R. Martz[1], Nichole N. Price[1,4], and Jennifer E. Smith[1]

[1]Scripps Institution of Oceanography, University of California San Diego, La Jolla, California, USA, [2]Department of Global Ecology, Carnegie Institution for Science, Stanford, California, USA, [3]Lamont Doherty Earth Observatory, Earth Institute at Columbia University, Palisades, New York, USA, [4]Bigelow Laboratory for Ocean Sciences, East Boothbay, Maine, USA, [5]Ecology and Evolutionary Biology, University of Santa Cruz, Santa Cruz, California, USA

Key Points:
- We present an autonomous approach to measure coral reef net calcification and production rates
- Net community production and calcification are coupled on time scales from minutes to days
- Available light is the primary driver for net community calcification (NCC); no relationship between Ω and NCC was observed

Correspondence to:
Y. Takeshita,
ytakeshita@carnegiescience.edu

Citation:
Takeshita, Y., W. McGillis, E. M. Briggs, A. L. Carter, E. M. Donham, T. R. Martz, N. N. Price, and J. E. Smith (2016), Assessment of net community production and calcification of a coral reef using a boundary layer approach, *J. Geophys. Res. Oceans*, *121*, 5655–5671, doi:10.1002/2016JC011886.

Received 14 APR 2016
Accepted 23 JUN 2016
Accepted article online 15 JUL 2016
Published online 10 AUG 2016

Abstract Coral reefs are threatened worldwide, and there is a need to develop new approaches to monitor reef health under natural conditions. Because simultaneous measurements of net community production (NCP) and net community calcification (NCC) are used as important indicators of reef health, tools are needed to assess them in situ. Here we present the Benthic Ecosystem and Acidification Measurement System (BEAMS) to provide the first fully autonomous approach capable of sustained, simultaneous measurements of reef NCP and NCC under undisturbed, natural conditions on time scales ranging from tens of minutes to weeks. BEAMS combines the chemical and velocity gradient in the benthic boundary layer to quantify flux from the benthos for a variety of parameters to measure NCP and NCC. Here BEAMS was used to measure these rates from two different sites with different benthic communities on the western reef terrace at Palmyra Atoll for 2 weeks in September 2014. Measurements were made every ~15 min. The trends in metabolic rates were consistent with the benthic communities between the two sites with one dominated by fleshy organisms and the other dominated by calcifiers (degraded and healthy reefs, respectively). This demonstrates the potential utility of BEAMS as a reef health monitoring tool. NCP and NCC were tightly coupled on time scales of minutes to days, and light was the primary driver for the variability of daily integrated metabolic rates. No correlation between CO_2 levels and daily integrated NCC was observed, indicating that NCC at these sites were not significantly affected by CO_2.

1. Introduction

Coral reefs are threatened worldwide from both local (e.g., overfishing, pollution, and sedimentation) and global (e.g., sea level rise, temperature, and ocean acidification) stressors. Therefore, there is a need to develop tools that can readily monitor reef health and ecosystem processes, beyond basic visual assessments, under natural conditions. Net community production (NCP) and net community calcification (NCC) are fundamental parameters that describe the carbon cycling of a reef. NCP describes the balance of organic production and respiration, and NCC describes the balance of calcification and dissolution. In particular, sustained measurements of NCC are of great interest, as this describes whether or not the reef is accreting biogenically precipitated $CaCO_3$, or if it is exhibiting a net loss of $CaCO_3$ through dissolution over time (although it does not capture other important processes such as bioerosion and mechanical wave erosion). Because ocean acidification is expected to cause NCC to decrease in the future [*Langdon et al*., 2000; *Doney et al*., 2009; *Andersson and Gledhill*, 2013; *Shaw et al*., 2015], there is a need to gain a better understanding of current rates and variability across time and space. A recent field manipulation experiment demonstrated that ocean acidification has already caused a ~12% decline in reef NCC since preindustrial times [*Albright et al*., 2016]. However, approaches that measure NCC are currently limited to those that require collecting discrete water samples, which are labor and time intensive, making it difficult to perform sustained observations. This sampling limitation is problematic, as variability in NCC on seasonal [*Bates et al*., 2010; *Falter et al*., 2012] to interannual [*Yeakel et al*., 2015] time scales has been observed. Quantifying and understanding the drivers of this variability is critical to establishing robust relationships between reef NCC and the progression of ocean acidification.

The ratio of NCC to NCP has been proposed as a valuable indicator for monitoring reef health [*Albright et al*., 2013; *Andersson and Gledhill*, 2013], as this ratio seems to be driven by the relative proportion of calcifying to noncalcifying organisms in the benthic community. For example, significantly higher ratios of NCC to NCP were observed over a coral and algal dominated reef flat relative to an algal dominated reef flat [*Smith*, 1973]. Further, because degradation of benthic reef communities is associated with a shift in dominance from corals to macroalgae [*Done*, 1992; *McCook*, 1999; *Nyström et al*., 2000; *McManus and Polsenberg*, 2004; *Hughes et al*., 2007] or more broadly from reef-building organisms (e.g., calcifiers) to fleshy organisms [*Smith et al*., 2016], the ratio of NCC to NCP could provide valuable insight into the functioning of these different communities. As most assessments of reef health focus on abundance estimates and descriptions of community structure, we do not have a good understanding of how variable these rates are across space and over time within and among communities. An approach that simultaneously and autonomously measures these two parameters would be a useful tool for monitoring reef health to inform management.

Autonomous measurements of net community production on coral reefs under in situ conditions have been achieved using three techniques: (1) control volume, (2) eddy covariance, and (3) gradient flux. The control volume is a modified Eularian approach which is capable of measuring subhourly metabolic rates over large patches of reef. Continuous measurements of NCP over weeks in Kaneohe Bay, O'ahu, Hawaii, documented large variability in daily production rates, ranging from net autotrophy to net heterotrophy [*Falter et al*., 2008]. Such dynamic variability could only be observed through sustained observations for multiple days. This same approach was used to measure NCC on an Australian fringing reef [*Falter et al*., 2012], however, discrete samples for total alkalinity (TA) were collected manually because autonomous sensors for TA are not currently available. Attempts have been made to pump water from the corners of the control volume and use bench-top instruments on a raft to measure dissolved inorganic carbon (DIC) and TA to overcome this limitation, yet the smaller dimensions required for this approach made it difficult to calculate robust metabolic rates [*Teneva et al*., 2013; *Koweek et al*., 2015].

The eddy covariance approach has been used in terrestrial environments for over half a century [*Montgomery*, 1948; *Swinbank*, 1951], and was introduced to the marine environment about a decade ago to measure benthic oxygen fluxes [*Berg et al*., 2003]. Since its introduction, it has been utilized to measure O_2 fluxes in a variety of ecosystems including on ice edges [*Long et al*., 2012b], in seagrass beds [*Long et al*., 2015b], and on coral reefs [*Long et al*., 2013]. However, due to stringent limitations on sensor performance, applications have thus far been largely limited to O_2 fluxes, though successful implementation for other parameters such as nitrate and pH have been reported [*Johnson et al*., 2011; *Long et al*., 2015a].

The gradient flux approach measures the mean gradient in momentum and chemical properties of interest in the benthic boundary layer (BBL) to calculate the bottom flux. This approach has been successfully applied in reef environments to quantify momentum [*Reidenbach et al*., 2006], phytoplankton [*Genin et al*., 2002], and O_2 fluxes (thus NCP) [*McGillis et al*., 2011; *Turk et al*., 2015]. The NCP rates based on this approach have been shown to agree well with estimates based upon closed in situ benthic enclosures [*Yates and Halley*, 2003, 2006; *Yates et al*., 2007]. However, the enclosure approach can require significant maintenance and multiple large-scale deployments. Enclosures also can become depleted of oxygen and nutrients if resupply is not managed. Here we propose that the gradient flux approach could be adopted to quantify benthic NCC, if gradients in TA could be observed or approximated.

Simultaneous measurements of pH and O_2 can be utilized to quantify perturbations to the carbonate system (i.e., TA and DIC) due to aerobic metabolism (photosynthesis and respiration) and other processes (e.g., anaerobic metabolism and/or calcification) [*Long et al*., 2015a]. In a coral reef community, the latter process can be assumed to be dominated by net calcification [*Barnes*, 1983; *Barnes and Devereux*, 1984]. Therefore, simultaneous pH and O_2 gradients in the BBL in a coral reef can be used to calculate a gradient in TA, thus NCC. Because autonomous sensing technology for O_2 and pH (the SeapHOx) are readily available for the oceanographic community [*Bresnahan et al*., 2014], these measurements can be easily made in situ.

To obtain accurate measurements of reef metabolism, it is important to conduct studies under natural flow fields. Reef metabolism is heavily influenced by flow, as it has been demonstrated that reef production is mass-transport limited [*Atkinson*, 1992; *Baird and Atkinson*, 1997; *Atkinson et al*., 2001; *Falter et al*., 2004]. Higher flow leads to a smaller diffusive boundary layer, promoting the transport of key constituents such as nutrients, carbon, and O_2 to and from the organism. Reduced flow under slack tide can lead to significantly

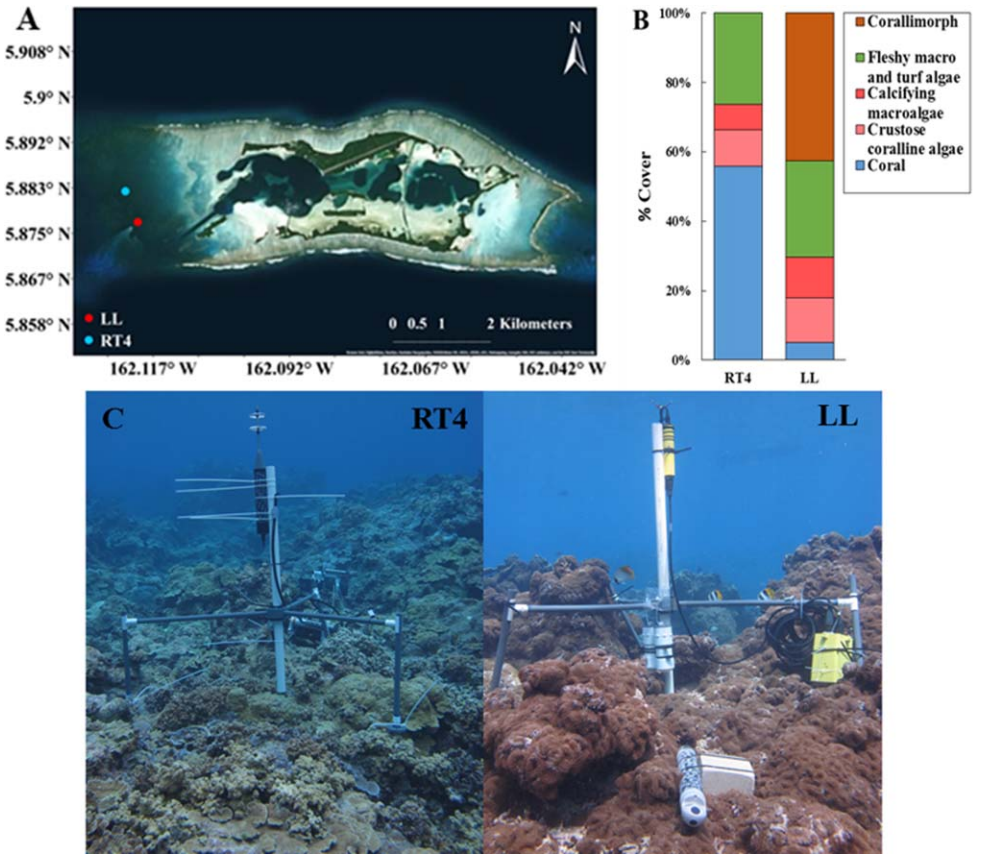

Figure 1. (a) Map of Palmyra. RT4 and LL is shown in blue and red, respectively. (b) Benthic community composition at RT4 and LL. (c) Picture of BEAMS at (left) RT4 and (right) LL. The vastly different benthic composition is clearly seen.

lower NCC [*Shaw et al*., 2014]. Flume experiments have demonstrated that flow can have significant impacts on how reef calcificers respond to ocean acidification [*Anthony et al*., 2011; *Comeau et al*., 2014].

Here we present the Benthic Ecosystem and Acidification Measurement System (BEAMS), an approach that is capable of simultaneously measuring benthic NCP and NCC at 10 minute intervals under natural flow conditions. BEAMS uses autonomous sensors to quantify mean gradients of pH and O_2 and the current velocity profile in the BBL to calculate benthic fluxes of O_2 (NCP) and TA (NCC). A 2 week time series of subhourly, in situ benthic NCP and NCC is presented from two sites with differing benthic communities on the reef terrace at the remote central Pacific Palmyra Atoll. We expected higher NCC rates at the site with the higher abundance of calcifying benthic taxa. The potential utility for BEAMS as a reef health monitoring tool is assessed by comparing metabolic rates under natural conditions simultaneously between two sites with vastly different benthic communities. Coupling between NCP and NCC on time scales of hours to days is discussed.

2. Methods

2.1. Study Site and Benthic Community Composition Analysis

All research was conducted on the coral reefs of Palmyra Atoll located in the northern Line Islands, central Pacific, approximately 5°N, 150°W (Figure 1). Palmyra is a National Fish and Wildlife Refuge and part of the recently established Pacific Remote Island Areas National Marine Monument. Thus, all of Palmyra's natural resources are protected under federal law. Aside from military occupation of the atoll during the 1950s, Palmyra's ecosystems have not been exposed to local human impacts such as fishing or pollution. As such Palmyra's reefs are among some of the healthiest reefs in the United States with coral and crustose coralline algal cover exceeding as much as 50% of the benthos [*Smith et al*., 2016]. While most of the forereef habitats on Palmyra are highly exposed, making biogeochemical research challenging, the shallow reef terrace

is more protected making it an ideal location to conduct biogeochemical cycling and feedback studies. Much of the reef terrace habitat is dominated by reef-building corals (>60% cover) [*Hamilton et al*., 2014] aside from an area adjacent to a former shipwreck site (that was removed in 2013 after 22 years) that is currently dominated by an invasive corallimorph (noncalcifying cnidarian) [*Work et al*., 2008].

Two BEAMS were deployed on 7–23 September 2014 on the western terrace at sites less than 1 km apart but with vastly different benthic communities (Figure 1a). Given the proximity between the two sites, similar environmental conditions were expected (see section 3 for details). Therefore, the differences in metabolic rates between the two sites were assumed to be driven by the benthic community. At each location, a 10 × 10 m square was mapped with BEAMS at its centroid. Each side of the square ran along north-south or east-west axes and we used photoquadrats (0.9 m × 0.7 m) every 2 m along the perimeter to quantify benthic community structure. In addition, one 10 m transect was run midway through the square (north to south) at 5 m marks and photoquadrats were taken every 2 m. All benthic images were collected using a Cannon G15 camera. The photographs were analyzed using the image analysis software *Photogrid 1.0*, following protocols from *Smith et al*. [2016]. Briefly, 100 stratified random points were distributed across each photo and the benthic organism underneath each point was identified to the finest taxonomic resolution possible. After identification, percent cover data were separated into the following functional groups: hard coral, calcified macroalgae, crustose coralline algae (CCA), turf algae, and corallimorph (Figure 1b). The reef terrace site (RT4; 5.877°N 162.119°W) was on average ~7 m deep and hosted a benthic community with an abundant population of calcifying organisms, consisting of 53% coral, 10% CCA, 7% calcifying macroalgae (*Halimeda* and *Galaxaura*), and 25% fleshy macro and turf algae. The Longliner wreck site (LL; 5.883°N 162.122°W) was on average ~6 m deep and was dominated by a large population of the corallimorph *Rhodactis howesii* (43%), 5% coral, 13% CCA, 12% calcifying macroalgae, and 28% fleshy macro and turf algae. The ship wreck was removed from the reef in 2013, a year prior to this deployment. Given the vastly different benthic communities at these two sites in terms of abundance of calcifying versus fleshy taxa, we expected higher NCC rates at RT4. However, as corallimorphs have symbiotic zooxanthellae for photosynthesis, comparable NCP rates were expected. Measurements were made at both sites for 14 days. A large swell event occurred on 12–13 September and mixed the water column thoroughly, thus metabolic rates were not calculated during this time. Three BEAMS were deployed on a single frame at RT4 for 24 h between 23 and 24 September to assess the reproducibility of this approach.

2.2. BEAMS Approach and Apparatus

BEAMS is based on the gradient flux approach, where vertical gradients in velocity and chemical constituents in the benthic boundary layer (BBL) are used to calculate chemical fluxes from the benthos [*McGillis et al*., 2011]. Gradients of O_2 are directly measured, whereas the gradient in TA is calculated using simultaneous measurements of pH and O_2. The flux of O_2 and TA from the benthos is directly proportional to benthic NCP and NCC, respectively, assuming negligible productivity in the BBL and no horizontal advective fluxes. The flux from the benthos (J) is equal to the product of the eddy diffusivity (Kz) and the vertical gradient of the chemical constituent C (i.e., O_2 or TA):

$$J = -K_z \frac{\partial C}{\partial z} \tag{1}$$

In a turbulent boundary layer, $K_z = \kappa u_* z$, where u_* is the friction velocity (m s^{-1}), κ is the Kármán constant (0.41), and z is the height above the benthos (m). Integrating equation (1) and rearranging gives:

$$C(z) = -\frac{J}{u_* \kappa} \ln\left(\frac{z}{d}\right) + C_1 \tag{2}$$

where d is the displacement height, and C_1 is the constant from integration. Measurements of the current profile in the BBL were used to quantify u_*, and three parameters (J, d, and C_1) were adjusted to fit the observations of the chemical constituents in the BBL using a nonlinear least squares approach (Matlab, lsqcurvefit). Net metabolic rates were calculated from the fluxes as NCP = J_{O2}, and NCC = $-0.5J_{TA}$, where the subscripts refer to the respective chemicals. NCP and NCC are reported in mmol O_2 m^{-2} h^{-1} and mmol $CaCO_3$ m^{-2} h^{-1}, respectively. Daily integrated NCP (mmol O_2 m^{-2} d^{-1}) and NCC ($CaCO_3$ m^{-2} d^{-1}) will be noted as ΣNCP and ΣNCC, respectively.

The chemical gradient in the BBL was measured using a SeapHOx [*Bresnahan et al*., 2014]. Gradients were measured using a single sensor by sequentially pumping water from different heights above the benthos through the SeapHOx. Separate pumps (Seabird SBE5P or Rule 25D bilge pumps) were used for the different heights, and a one-way valve was attached at each inlet. Water was pumped continuously from each height for 15 min before switching to the next height. The SeapHOx made measurements every 45 s. A single sensor approach is advantageous over multiple sensors when monitoring small chemical gradients, as the measurements rely on the precision of one instrument. Using this approach, we largely alleviate complications that arise when using multiple sensors, namely intra sensor offset or bias. The short-term precision of pH and O_2 is 0.0005 [*Martz et al*., 2010; *Takeshita et al*., 2014] and 0.1 μmol kg^{-1}, respectively. Data from the first 2 minutes after switching intakes were discarded to ensure full flushing of the sample volume, and remaining data were averaged to obtain the mean chemical gradient over the sampling period ($n = 18$). The pH measurements were calibrated based on discrete samples for DIC and TA taken alongside the sensor throughout the deployment ($n \geq 12$ for each sensor), and the accuracy of the sensor pH is estimated to be 0.01 based on this comparison. pH at in situ conditions was calculated using CO2SYS with equilibrium constants based on measurements by *Mehrbach et al*. [1973] and refit by *Lueker et al*. [2000]. All pH is reported at in situ conditions, on the total scale.

The gradient in TA ($\Delta TA = TA_{z2} - TA_{z1}$) was estimated using pH and O_2 data [*Barnes*, 1983]:

$$-\Delta TA = \frac{(\Delta O_2 \times Q + (K_{z1} - K_{z2})TA_{z2} - K_{z1}(B_{z1} + OH_{z1}) + K_{z2}(B_{z2} + OH_{z2}))}{(K_{z1} - 0.5)} \quad (3)$$

where $\Delta O_2 = O_{2,z2} - O_{2,z1}$, Q describes the change in DIC per change in O_2 due to net production ($\Delta DIC/\Delta O_2$), K is the ratio of carbonate alkalinity to DIC, B is the borate concentration (μmol kg^{-1}), and OH is the hydroxide concentration, and the subscript denotes the height above the benthos ($z_1 = 0.3$ m and $z_2 = 1.1$ m). Borate concentration was calculated from salinity [*Uppstrom*, 1974] and equilibrium constants from *Dickson* [1990], OH was calculated using pH and K_w [*Millero*, 1995], and K was calculated from temperature, salinity, and pH [*Barnes*, 1983]. Note that Q is the inverse of the photosynthetic quotient. TA_{z2} was assumed to be 2205 μmol kg^{-1} (mean of discrete TA samples; $n = 35$), since the calculations are relatively insensitive to the choice in this value. In fact, changing TA_{z2} by ±100 μmol kg^{-1} (larger than the range observed from discrete samples) resulted on average a difference of ΔTA of ±0.3 μmol kg^{-1}. This propagated out to an uncertainty of 0.5–2 mmol $CaCO_3$ m^{-2} h^{-1} (up to 14% of the mean daily maximum NCC at RT4) depending on the flow; error is higher at higher flow. Here we assumed a Q of 1 (see section 4.1 for details).

The velocity profile of the BBL with a vertical resolution of 3 cm was measured using a Nortek 2 MHz HR Aquadopp at 1 Hz. Assuming a no-slip boundary condition and a law of the wall relationship, the velocity profile can be expressed as

$$U(z) = \frac{u_*}{\kappa} \ln\left(\frac{z-d}{z_o}\right) \quad (4)$$

where U is the current velocity, d is the displacement height, and z_o is the roughness scale. The friction velocity, u_*, was obtained by fitting equation (4) to the observed current profile by adjusting u_*, d, and z_o using nonlinear least squares (MATALB function lsqcurvefit); mean velocity profiles over 5 min were used for this fit. Due to instrumentation limitation, the current profile was not continuously measured at both sites. Alternatively, velocity at 1.3 m (U_0) was measured at 0.1 Hz using a Sontek Acoustic Doppler Velocimeter (LL) and a Nobska MAVS (RT4), and u_* was calculated based on a linear relationship between U_0 and u_* ($R^2 > 0.96$ for both sites). The drag coefficient (C_d) was calculated for each site. All regression analysis was performed using MATLAB, using lsqfitma and regress functions for model II and least squares regressions, respectively. The footprint, or the benthic area that is responsible for fluxes calculated by BEAMS can be represented by $u_*/z = U(z)/L$, where L is the footprint length [*McGillis et al*., 2011].

A diel composite plot for hourly NCC and NCP was created by averaging hourly binned metabolic rates over the deployment. NCC, NCP, and daily integrated PAR (ΣPAR) were calculated on days where data from the entire 24 h were available ($n = 7$ and $n = 8$ for LL and RT4, respectively). Gross primary production (GPP) was calculated following the approach outlined in *Falter et al*. [2012].

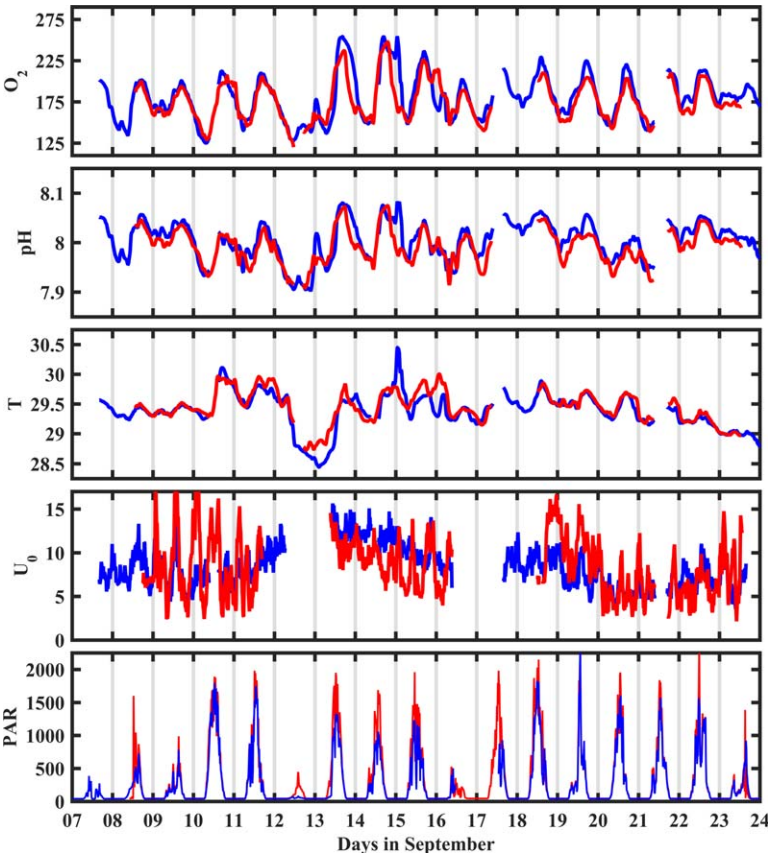

Figure 2. Time series of O_2 (μmol kg^{-1}) pH, temperature (°C), current velocity (U_0; cm s^{-1}), and PAR (μmol photons m^{-2} s^{-1}) from RT4 (blue) and LL (red). Data are from 1.1 m above the benthos. Gaps in data are due to sensor maintenance.

Photosynthetically active radiation (PAR) was estimated by measuring irradiance at each site using an Onset HOBO irradiance logger. A LICOR 4-π quantum sensor that measured PAR was deployed alongside each of the HOBO loggers for >1 day, and irradiance (lumen) was converted to PAR (μmol photons m^{-2} s^{-1}) using an exponential function ($R^2 > 0.86$ for both sites) [*Long et al*., 2012a]. The surfaces of the irradiance loggers were cleaned every day by wiping with a neoprene glove.

2.3. Discrete Samples for DIC and TA

Discrete samples for DIC and TA were collected using both diver deployed Niskin bottles and autosamplers. Samples from Niskin bottles were collected and analyzed following standard protocols [*Dickson et al*., 2007]. Autosamplers were custom built, and consisted of a peristaltic pump that filled a 350 mL prepoisoned intravenous bag resistant to gas exchange (Tedlar, Zefon EconoGrab^{TM}) over 15–20 min. The bags were collected daily and siphoned into 300 mL borosilicate bottles. The autosamplers were programmed to collect samples at either 1 or 11 A.M. each day, local time. Duplicate samples using the autosamplers agreed to better than 2.5 μmol kg^{-1} for both TA and DIC ($n = 4$). The samples were analyzed in the Dickson lab at Scripps Institution of Oceanography, and the precision and accuracy for DIC and TA are estimated to be 1 and 2 μmol kg^{-1}, respectively. A total of 23 and 12 samples were collected at RT4 and LL, respectively. The saturation state with respect to aragonite (Ω) was estimated from sensor data based on a pH-Ω relationship established using the discrete samples (second-order polynomial; $R^2 = 0.999$). Ω estimates are accurate to 0.01.

3. Results

The two sites exhibited similar environmental conditions over the course of the deployment (Figure 2) as they were located ~1 km apart. Mean temperature was 29.6°C, and varied by <1°C, except for during a significant swell event occurring during 12–13 September, when temperatures decreased to 28.5°C. Clear diel

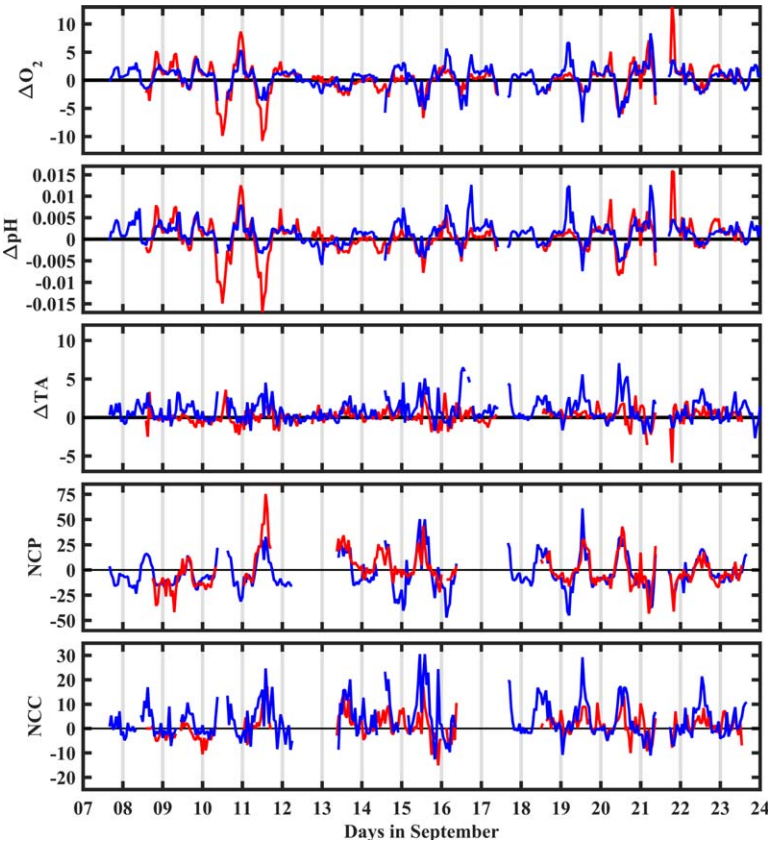

Figure 3. Time series of hourly binned ΔO_2 (μmol kg^{-1}) ΔpH, ΔTA (μmol kg^{-1}), NCP (mmol O_2 m^{-2} h^{-1}), and NCC (mmol $CaCO_3$ m^{-2} h^{-1}) from RT4 (blue) and LL (red). Gaps in data are due to sensor maintenance or unfavorable flow conditions.

cycles of O_2 and pH were observed at both sites, and the daily range was approximately 70 μmol kg^{-1} and 0.1 for O_2 and pH, respectively. The current velocity showed similar general patterns between the two sites, however, short-term variability was greater at LL, which was dominated by fleshy organisms, compared to RT4 that is dominated by calcifiers. The drag coefficient, C_d, for each site was 0.019 ± 0.02 ($R^2 > 0.96$ for both sites), based on U_0 and u_* determined from the current profile. These values are similar to those reported by *McGillis et al*. [2011], but slightly higher than *Reidenbach et al*. [2006]. The footprint length, L, was 10.1 m for both sites. Sunrise and sunset occurred during this deployment around 6:30 A.M. and 7:00 P.M., respectively.

A consistent, repeatable diel pattern in ΔO_2, ΔpH, and ΔTA was observed reflecting cycles of reef metabolism (Figure 3). Negative and positive ΔO_2 were observed during the day and at night, respectively; negative ΔO_2 means the O_2 closer to the benthos is higher, signifying positive NCP, and vice versa. ΔpH followed a very similar pattern to ΔO_2, indicating that the pH gradient is dominantly driven by NCP. Clear gradients in TA reflecting NCC were observed at RT4 (i.e., positive ΔTA for positive NCC), whereas no clear diel pattern in ΔTA was observed at LL (Figure 3), likely because this site is dominated by noncalcifying benthic organisms. An exception to this pattern was observed on 12–13 September, when no significant chemical gradient was observed throughout the day. This was most likely due to low PAR associated with the storm event, and very large swells and breaking waves on the reef terrace, inducing high mixing that led to a well-mixed water column and a small BBL; NCC and NCP could not be calculated for those days.

A total of 1144 and 1018 NCC and NCP rates were calculated at RT4 and LL using equation (2) over 2 weeks, respectively (Figure 3). Gaps in the benthic flux time series were due to unfavorable conditions (e.g., 12–13 September), when the BBL was stratified, or during instrument maintenance to replace batteries. A diel composite of the metabolic rates showed consistent diel patterns of positive NCP during the day and negative NCP during the night at both sites (Figure 4). A clear diel cycle for NCC was observed at RT4, where NCC was positive during the day, and remained near zero during the night (Figure 4). However, at LL where

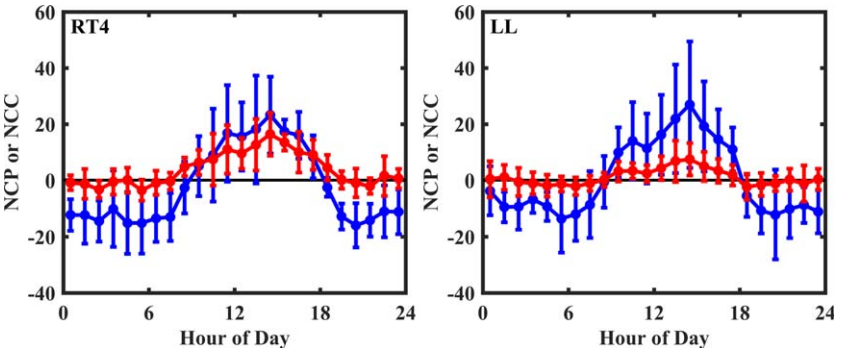

Figure 4. Diel composite plot of hourly NCP (blue; mmol O_2 m^{-2} h^{-1}) and NCC (red; mmol $CaCO_3$ m^{-2} h^{-1}) for RT4 and LL. Error bars are 1 SD; note that the error bars reflect day-to-day variability.

noncalcifying organisms dominate, this pattern was far less pronounced (Figure 4). On average, the diel maximum NCP was similar at both sites (~23 mmol O_2 m^{-2} h^{-1}), whereas the average daily maximum NCC rate was twice as high at RT4 (14 mmol $CaCO_3$ m^{-2} h^{-1}) than at LL (6 mmol $CaCO_3$ m^{-2} h^{-1}). Based on the integral of this diel composite plot, the average ΣNCP was −34 mmol O_2 m^{-2} d^{-1} (RT4) and 22 mmol O_2 m^{-2} d^{-1} (LL), and the average ΣNCC was 95 mmol $CaCO_3$ m^{-2} d^{-1} (RT4) and 26 mmol $CaCO_3$ m^{-2} d^{-1} (LL). However, large variability in ΣNCP and ΣNCC was observed at both sites (Table 1). Both sites exhibited net autotrophy and net heterotrophy over the course of a day; ΣNCP ranged between −169 and 94 mmol O_2 m^{-2} d^{-1} at RT4, and ranged between −217 and 318 mmol O_2 m^{-2} d^{-1} at LL. Over a diel cycle, RT4 was always net calcifying (ΣNCC ranging between 50 and 159 mmol $CaCO_3$ m^{-2} d^{-1}), whereas net dissolution was observed 1 day at LL, most likely due to low light levels that day.

Both NCP and NCC were correlated with PAR (Figure 5). A community-level Photosynthesis-Irradiance (P-I) curve was determined using a simple exponential equation, assuming no photoinhibition [*Platt et al*., 1980]

$$NCP = P_{max}\left(1 - e^{\frac{-\alpha_P \times PAR}{P_{max}}}\right) - C_P \quad (5)$$

where α_P is the photosynthetic efficiency, P_{max} is the maximum NCP, and C_P is a constant. Both α_P and P_{max} were very similar between the two sites (Table 2). NCC had a similar response to light, thus the same form of equation was used to fit the data to create a Calcification-Irradiance curve (Figure 5). Both the initial slope (α_G) and maximum (G_{max}) were higher at RT4 compared to LL (Table 2). Both NCP and NCC responded to changes in PAR on time scales faster than the sampling interval of ~15 min. For example, a cloud-induced decrease in PAR around noon on 15 September led to rapid and dramatic decreases in both NCP and NCC (Figure 6). In fact, negative NCP was briefly observed during the middle of the day, demonstrating the need for high-frequency measurements to capture the dynamic variability of reef metabolism.

Table 1. ΣNCP (mmol O_2 m^{-2} d^{-1}), ΣNCC (mmol $CaCO_3$ m^{-2} d^{-1}), ΣPAR (mol photons m^{-2} d^{-1}), and Mean Daily Average Ω

	ΣNCP		ΣNCC		ΣPAR		Ω	
Day in September	RT4	LL	RT4	LL	RT4	LL	RT4	LL
8	−118		101		8.5		3.49	
9	−169	−217	76	−36	7.4	9.1	3.20	3.46
10		318		32		36.8		3.17
11	41		120		25.4		3.60	
14		118		42		26.2		3.58
15	94	79	219	8	21.1	27.8	3.58	3.59
18	33		114		29.9		3.59	
19	−101	15	117	58	19.6	19.5	3.47	3.21
20	66	23	92	28	23.3	25.5	3.44	3.46
22	22	−37	106	39	24.3	28.7	2.82	3.05
Average[a]	−16	43	118	18	19.9	24.8	3.29	3.36
SD	98	162	43	27	8.0	8.6	0.26	0.21

[a]The average for ΣNCP and ΣNCC was computed as the integral from the curve in Figure 4.

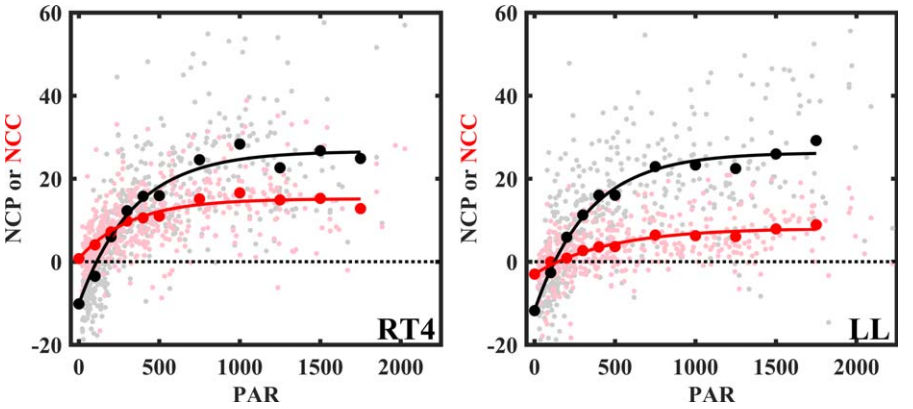

Figure 5. PAR (μmol photons m^{-2} s^{-1}) versus NCP (black; mmol O_2 m^{-2} h^{-1}) and NCC (red; mmol $CaCO_3$ m^{-2} h^{-1}) at (left) RT4 and (right) LL. R^2 for NCP and NCC at RT4 was 0.57 and 0.35, respectively, and R^2 for NCP and NCC at LL was 0.61 and 0.45, respectively. Individual BEAMS measurements and binned averages are shown in shaded and solid circles, respectively. The solid lines represent the best fit line, and the dashed line represents zero. Both NCP and NCC follow an exponential relationship to PAR.

A tight relationship between NCP and NCC was observed during the day (defined as PAR > 100 μmol photons m^{-2} s^{-1}) at both sites (Figure 7). The ratio of NCC to NCP was significantly higher (*t* test; $p < 0.001$) at RT4 (0.50 ± 0.02) relative to LL (0.27 ± 0.01), and this ratio remained consistent throughout the deployment. This correlation existed between daily integrated rates as well (Figure 8), but the ratio of ΣNCC to ΣNCP was lower (0.37 ± 0.08 at RT4 and 0.21 ± 0.08 at LL) compared to patterns shown in Figure 7. ΣNCP and ΣNCC were also correlated to ΣPAR, however, no clear relationship between ΣNCC and the daily average Ω was observed (Figure 8).

4. Discussion

4.1. BEAMS Approach and Assessment

The footprint length, L, of the reef that influences the observations at each site was estimated to be approximately 10 m, thus the metabolic fluxes should reflect the benthic community near each system. At RT4, >70% of the benthos is covered by calcifying photoautotrophs (e.g., corals and calcifying algae), whereas at LL, the benthos is dominated by *R. howesii* (a noncalcifying photosymbiotic corallimorph) and fleshy turf algae, and calcifiers composed only 30% of the community. Accordingly, the ratio of NCC to NCP at RT4 (0.50 ± 0.02) was greater than at LL (0.27 ± 0.01) (Figure 7), indicating higher calcification rates at RT4; ΣNCC was approximately 3.5 times larger at RT4 (Table 1). These data demonstrate that BEAMS captured metabolic patterns that are consistent with visual assessments of the composition of the underlying benthic community.

NCC at RT4 was generally within the range of previously reported values over the western reef terrace using a Lagrangian approach, which ranged between −50 and 100 mmol $CaCO_3$ m^{-2} h^{-1} [*Koweek et al.*, 2015]. Measurements in *Koweek et al.* [2015] were performed during the same time of year, and the environmental conditions (e.g., PAR and temperature) were similar to those observed during this study. However, this could be due to the large uncertainties associated with Lagrangian measurements. *Koweek et al.* [2015] also measured NCC using a Eularian approach for the southwestern portion of the reef terrace several kilometers from RT4, and reported rates significantly higher than our study. For example, NCC was on average larger by about 15–20 mmol $CaCO_3$ m^{-2} h^{-1}, with ΣNCC of >650 mmol $CaCO_3$ m^{-2} d^{-1}, over 5 times greater than our estimates. The discrepancy could be driven by different benthic communities, spatial variability in reef metabolic rates, or different flow regimes. Although reef terraces are very distinct from reef flats, for a global context, we note that the NCC at RT4 (3.6 kg $CaCO_3$ m^{-2} yr^{-1}) is about 90% of the average NCC (~4 kg $CaCO_3$ m^{-2} yr^{-1}) for reef flats in the Indo-Pacific [*Kinsey*, 1985; *Falter et al.*, 2013]. The ratio

Table 2. Coefficients for P-I and C-I Curve for Both Sites

Coefficients	RT4	LL
α_P	0.107	0.113
P_{max}	36.8	38.1
C_P	−10.1	11.8
α_G	0.045	0.024
G_{max}	14.4	11.1
C_G	1.89	−1.61

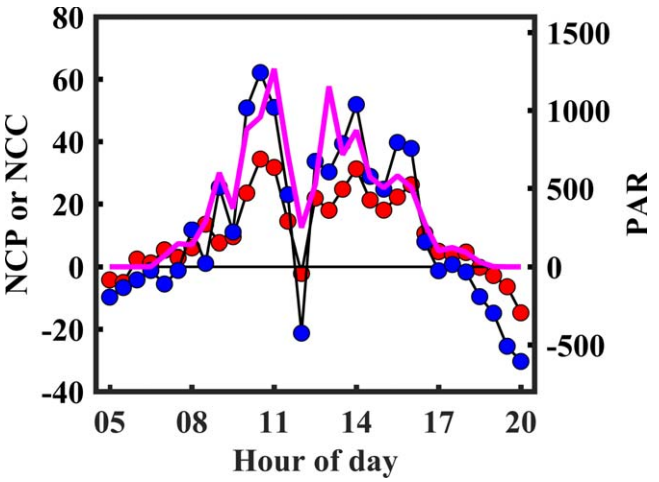

Figure 6. Daytime NCP (blue; mmol O_2 m^{-2} h^{-1}) and NCC (red; mmol $CaCO_3$ m^{-2} h^{-1}) on 15 September at RT4. PAR (μmol photons m^{-2} s^{-1}) is shown as a solid pink line, demonstrating the coupling between PAR and reef metabolism on time scales of tens of minutes.

of NCC to NCP (0.50) is one of the highest reported in the literature, although this number varies depending on the assumption of Q.

The accuracy of the gradient flux approach is dependent on the ability to quantify the chemical gradients in the BBL, which are typically smaller than 3 μmol kg^{-1} O_2 and 0.005 pH. To achieve this level of resolution, there are several considerations that need to be taken into account. First, measurement precision must be significantly smaller than the expected gradient, indicating that high-precision autonomous sensors are necessary. We recommend using a single sensor approach to eliminate measurement uncertainty resulting from intersensor accuracy (e.g., calibration errors and sensor drift). Our attempts at collecting discrete samples to quantify the chemical gradient have not been successful, as the sampling uncertainties were too large. Second, the gradient flux approach requires that the mean chemical conditions are measured at each height. In a turbulent boundary layer, eddies transport water parcels vertically on time scales ranging from fractions of seconds to multiple seconds [*Berg et al.*, 2003], resulting in natural variability at a fixed height. For example, the average standard deviation of O_2 and pH at each height over the course of 15 min was 0.6 μmol $kg^{-1}$and 0.001, respectively. While part of this variability stems from instrument precision, it largely reflects the turbulent processes in the BBL. Therefore, it is critical that a sufficient number of measurements are averaged to remove the high-frequency variability. For more recent deployments, we have started averaging measurements for 10 min at each height.

The random error associated with the calculation of ΔTA was assessed. The error associated with Q was not included in this analysis because this represents a systematic bias, but is discussed in detail below. The sources of random error that were considered are summarized in Table 3. The contribution of each source of error was determined using a Monte Carlo approach, and is reported as the standard deviation of 1000 simulations. Errors were introduced into the simulation by assuming a random distribution. The three main sources of uncertainty were the instrumental precision in O_2 (±0.2 μmol kg^{-1}) and pH (±0.6 μmol kg^{-1}), and the assumption in TA_{z2} (±0.3 μmol kg^{-1}), with a total random error of ±0.86 μmol kg^{-1}. This corresponds to a random error in NCC of 1.5 to 6 mmol $CaCO_3$ m^{-2} h^{-1} (up to 45% of mean daily maximum NCC at RT4) depending on the current velocity. The uncertainty due to the assumption of TA_{z2} can be greatly reduced by simultaneously deploying an autonomous sensor for another carbonate parameter (e.g., pCO_2). However, combining pH and pCO_2 sensors to measure the TA gradient in the BBL is not recommended. The random error in the calculated ΔTA if pH and pCO_2 were used is ±4.5 μmol kg^{-1}, assuming a sensor precision of 0.0005 and 1 μatm, 27°C, and salinity of 33.5. As this error is larger than most of the gradients in TA we observed, we do not believe that robust NCC rates

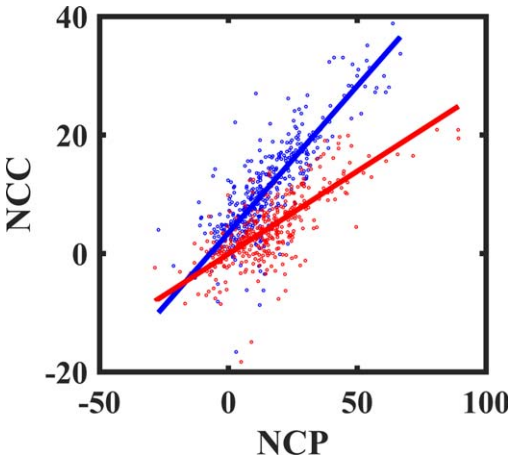

Figure 7. Daytime NCP (mmol O_2 m^{-2} h^{-1}) versus NCC (mmol $CaCO_3$ m^{-2} h^{-1}) at RT4 (blue) and LL (red). Solid lines represent model II regression results. Slope at RT4 and LL were 0.50 ± 0.02 (R^2 = 0.66) and 0.27 ± 0.01 (R^2 = 0.54), respectively, demonstrating higher calcification rates at the healthy reef site RT4, and a consistent NCP to NCC ratio at both sites.

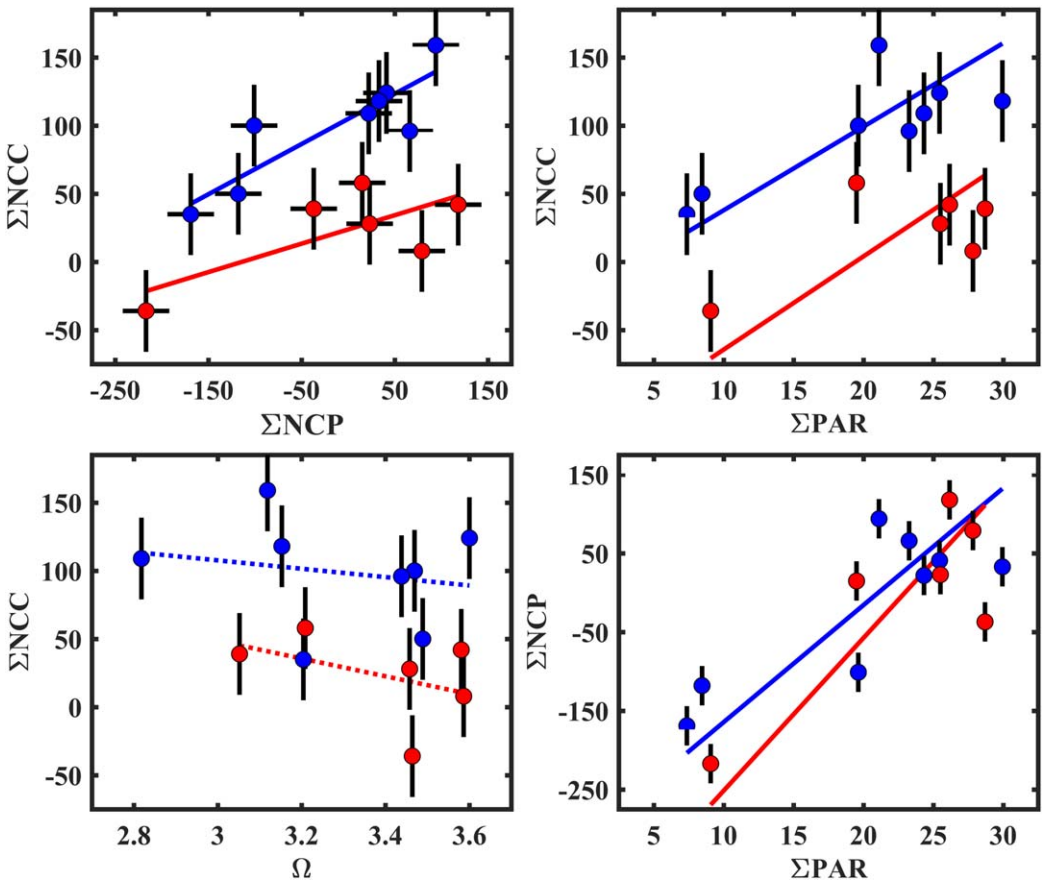

Figure 8. Relationship between ΣNCP (mmol O_2 m^{-2} d^{-1}), ΣNCC (mmol $CaCO_3$ m^{-2} d^{-1}), ΣPAR (mol photons m^{-2} d^{-1}), and daily average Ω at both sites. Data from RT4 and LL are shown in blue and red, respectively. Error bars represent uncertainty in the daily integrated metabolic rates. Solid lines represent model II regression results where the slope was significant at the 0.05 level. Dashed lines indicate a nonsignificant slope.

can be obtained with this sensor combination. It is unlikely that the precision of pH and O_2 sensors will significantly improve, as they are comparable to standard bench-top systems.

The theoretical random error propagation of BEAMS was assessed by simultaneously deploying three systems on the same frame for 24 h on 22–23 September. The discrepancy between the three systems should reflect the random error of BEAMS in the field. On average, the NCP and NCC from the three systems agreed to 2.4 and 3.2 mmol C m^{-2} h^{-1}, computed as the standard deviation of the three metabolic fluxes from the different systems (Figure 9). The field observations are in general agreement with the calculated random error in NCC of 1.5–6 mmol $CaCO_3$ m^{-2} h^{-1}. This random error is significantly smaller than the metabolic fluxes observed during our study, thus robust estimates of metabolic fluxes were possible. Taking the reproducibility for hourly rates and propagating them to daily integrated metabolism rates leads to an approximate uncertainty in ΣNCP and ΣNCC of ±13 mmol O_2 m^{-2} d^{-1} and 15 mmol $CaCO_3$ m^{-2} d^{-1}, respectively. The scatter between the systems was almost entirely due to the differences in the captured chemical gradients. The agreement between the current sensors was

Table 3. Summary of the Sources and Magnitude of Random Error for ΔTA[a]

Source of Error	Magnitude	Propagated Error in ΔTA
O_2 precision (μmol kg^{-1})	0.1	0.20
pH precision	0.0005	0.58
Salinity precision	0.005	0.08
Temperature precision (°C)	0.005	0.09
pH accuracy	0.01	0.02
Salinity accuracy	0.005	0.00
Temperature accuracy (°C)	0.1	0.00
TA_{z2} (μmol kg^{-1})	100	0.26
K_1	1.92E-8	0.01
K_2	2.88E-11	0.01
Total		0.86

[a]Assumption in Q is not included in this table, as it is not random error.

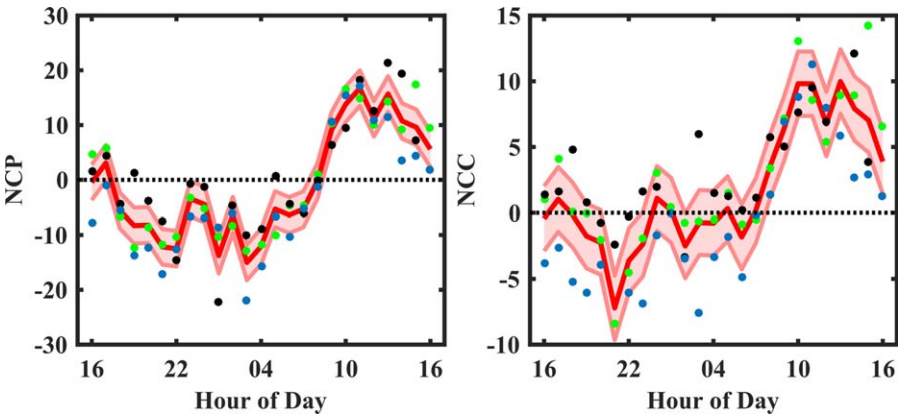

Figure 9. NCP and NCC calculated from three separate SeapHOx sensors simultaneously deployed at RT4. The mean ± SD of the three sensors are shown in red, whereas the individual measurements are shown in closed circles. Different colors indicate different BEAMS. The mean standard deviation for NCP and NCC was 2.4 mmol O_2 m^{-2} h^{-1} and 3.2 mmol $CaCO_3$ m^{-2} h^{-1}.

0.2 ± 0.4 cm s^{-1} and did not introduce significant uncertainty to the calculated metabolic fluxes. In the future, this error could potentially be improved by implementing different pumping flow rates or adjusting the number and frequency of measurements made at each height.

Another source of error to this approach is the assumption made for Q in equation (3). Unlike the sources of error considered earlier, the assumptions in Q manifest as a systematic error. In this study, we assumed $Q = 1$ because a review of reefs worldwide revealed that the photosynthetic quotient falls into a narrow range near unity [*Kinsey*, 1985], but ranges between 0.8 and 1.15. More recent studies have also shown that Q in reef environments was not significantly different than one [*Falter et al*., 2012]. We assessed how this assumption affects NCC at RT4 by altering Q between 0.9 and 1.1 (Figure 10). Lower Q increases nighttime NCC and decreases daytime NCC; the opposite occurs when Q is increased. Peak day time NCC at RT4 ranged between 13.3 ($Q = 0.9$) and 18.5 ($Q = 1.1$) mmol $CaCO_3$ m^{-2} h^{-1}, representing a ~20% systematic error. Since NCP is unaffected by the assumption in Q, this leads to a different ratio of NCC to NCP, in this case, between 0.38 ± 0.02 ($Q = 0.9$) and 0.58 ± 0.02 ($Q = 1.1$). It is clear that better constraining Q will lead to more accurate estimates of NCC, and should be a priority in future deployments. The daily integrated value is relatively insensitive to the choice in Q, and only varied by ±5 $CaCO_3$ m^{-2} d^{-1}. This is because the effects of Q during night and day (or more strictly negative and positive ΔO_2) are opposite, and work to counteract each other. This demonstrates that although hourly NCC may be sensitive to the choice in Q, the daily integrated NCC derived from BEAMS is robust. However, on higher-latitude reefs where the length of day and night are less balanced than low-latitude reefs, the daily integrated NCC may also be sensitive to Q, but has yet to be confirmed.

4.2. Drivers for NCC

4.2.1. Light

An exponential relationship between PAR and NCP is well established [*Platt et al*., 1980; *Gattuso et al*., 1996; *Long et al*., 2013; *Turk et al*., 2015], though there is less consensus on the shape of the relationship between PAR and NCC. Examples for linear [*Barnes and Devereux*, 1984; *Gattuso et al*., 1996; *Falter et al*., 2012; *Albright et al*., 2013] and exponential [*Gattuso et al*., 1996; *Boucher et al*., 1998; *Cuet et al*., 2011] relationships have been reported. Because NCC and NCP were tightly correlated at both RT4 and LL (Figure 7), it is logical to expect that the relationship between NCC and PAR would follow a similar shape as that of NCP and PAR (i.e., exponential; Figure 5), although some studies have hypothesized different sensitivities to PAR for NCP and NCC [*Shamberger et al*., 2011]. The different patterns in the literature could reflect different ecosystem behavior between reefs, or the spatial discrepancies between the different approaches. Most nonenclosure approaches to measure NCC (e.g., Lagrangian, Eularian, and control volume) integrate metabolic rates over wider areas than BEAMS. Alternatively, approaches that rely on discrete samples usually have sampling intervals of an hour to several hours, making it difficult to capture reef metabolic rates with sufficient temporal resolution to accurately capture the curvature at low PAR levels when light levels are rapidly changing (i.e., right after sunrise and before sunset). The BEAMS approach does not have this restriction, and is

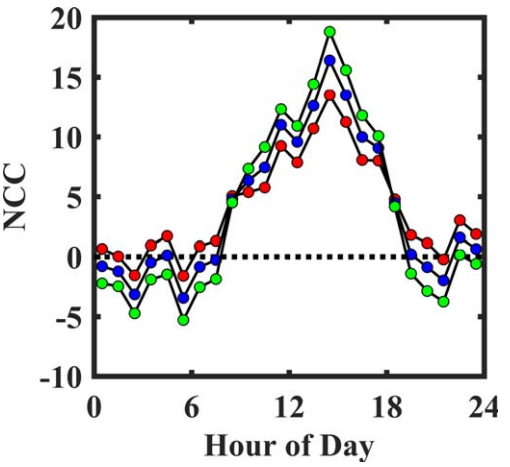

Figure 10. Diel composite of NCC (mmol $CaCO_3$ m^{-2} h^{-1}) for RT4 assuming a Q of 0.9 (red), 1.0 (blue), and 1.1 (green).

capable of detecting changes in metabolic rates on similar time scales as the changes in environmental conditions (Figure 6). Deployment of BEAMS in varying benthic communities and reef environments would shed light on this issue.

A decoupling between PAR and NCC has been observed in the laboratory for mixotrophic corals, where organisms followed a natural diel cycle independent of light [*Al-Horani et al*., 2007]. Similar observations have been made in the field. For example, *Falter et al*. [2012] observed rates of NCC that were higher than expected based on empirical light relationships on two anomalously low light days. They argued that this was due to the reef flat exhibiting a diurnal rhythm independent of diurnal change in light. Our observations do not support a circadian rhythm for reef NCC. The reef community responded rapidly to changes in incident light (Figure 6), and the total daily net calcification seems to be driven by the total amount of light for each day, as evidenced by the correlation between ΣPAR and ΣNCC (Figure 8). If reefs followed a circadian rhythm, no significant relationship should be observed between ΣPAR and ΣNCC. Alternatively, this may indicate a reef's relative dependence on autotrophic versus heterotrophic processes to build carbonate skeletons.

The ratio of ΣNCC to ΣNCP at RT4 (0.37 ± 0.07) and LL (0.20 ± 0.08) were similar to that obtained based on daytime data (Figure 6), suggesting that daily integrated metabolic rates are largely driven by day time production and calcification dynamics. This is further supported by the correlation between ΣNCC and ΣPAR, and ΣNCP and ΣPAR (Figure 8), as light has a strong control over day time metabolism. Therefore, the day-to-day variability in ΣNCC and ΣNCP are, on the first order, driven by the available light during that day. The observed variability in ΣNCC was large and it differed by threefold throughout the deployment at RT4. This highlights the importance of simultaneously reporting PAR with NCC rates for future reef calcification studies, especially if results are to be interpreted to detect temporal trends. For example, the natural variability in ΣNCC due to light levels is of similar or greater magnitude than the expected changes in NCC due to ocean acidification [*Langdon et al*., 2000; *Pandolfi et al*., 2011; *Chan and Connolly*, 2013; *Shaw et al*., 2015]. Therefore, any anthropogenically forced changes may become extremely difficult to detect because they may get lost in the noise of natural variability. Incorporation of PAR in the interpretation will become critical if meaningful changes are to be described or comparisons to be made within and among sites. It is important to note that seasonal changes in the response of ΣNCC to ΣPAR have been observed [*Falter et al*., 2012], making thorough characterization of each site critical. Although not included in this discussion, temperature also has an important control over NCC [*Silverman et al*., 2009]. Since our deployment sites did not experience a large temperature change (<1°C), we did not attempt to address the effects of temperature with our data. However, deployment of BEAMS in environments with large temperature variability or over multiple seasons will allow us to examine temperature effects on NCC.

4.2.2. Net Community Production

A strong correlation between NCC and NCP in reef environments is well documented [*Gattuso et al*., 1996; *Shaw et al*., 2012, 2015; *McMahon et al*., 2013; *Albright et al*., 2015], and was observed at both sites in this study (Figure 6). NCC was more strongly correlated to NCP ($R^2 = 0.66$) than PAR ($R^2 = 0.40$), further supporting the hypothesis that calcification is strongly driven by production [*Gattuso et al*., 1999]. The ratio was significantly higher at RT4, a "healthy" reef site with high abundance of coral and calcifying organisms, compared to LL, a degraded site dominated by invasive noncalcifying photosynthetic corallimorphs and fleshy turf algae (Figure 7). The difference in benthic community composition between these two sites is analogous to a reef transitioning from a coral to algal dominated state through various stressors. The large differences in the ratio of NCC to NCP observed across the two sites indicate that monitoring this ratio could be a powerful tool for monitoring reef health, as has been previously suggested [*Albright et al*., 2013; *Andersson and Gledhill*, 2013].

Previous studies have demonstrated that daily integrated gross primary production (ΣGPP) is significantly correlated to ΣNCC, however, ΣNCP and ΣNCC are not [*Kinsey*, 1985; *Gattuso et al*., 1999; *Shamberger et al*., 2011; *Falter et al*., 2013]. This is contrary to our results, where a correlation between both ΣGPP and ΣNCC ($R^2 = 0.63$ at RT4; data not shown), and ΣNCP and ΣNCC ($R^2 = 0.76$) existed (Figure 8). In fact, ΣNCC was more strongly correlated to ΣNCP than ΣGPP. One reason this relationship has not been shown in the past could be that continuous measurements of both NCP and NCC for multiple days must be made. Furthermore, the deployment should span a wide range of light levels to obtain robust regression analysis results. Such datasets are scarce [*Shamberger et al*., 2011]. Alternatively, this discrepancy could result from the exclusion of water column processes in NCP measured by the BEAMS approach. Previous approaches for quantifying reef metabolism using bulk seawater chemistry measure integrated metabolic rate of the benthos and water column. Water column processes, which are typically considered to be small or negligible in many reef systems, could introduce enough variance to convolute the relationship between the diel integrated metabolic rates.

4.2.3. Ω

No correlation was observed between daily average Ω and NCC (Figure 8), suggesting that Ω does not significantly affect NCC at these sites, or that the effects of Ω were too small to detect. This is contrary to a tight correlation between daily average Ω and ΣNCC that was previously reported from Kaneohe Bay [*Shamberger et al*., 2011], indicating that perhaps different reefs may be more sensitive to changes in Ω. However, such relationships must be interpreted with caution, as they could be an artifact of the feedback of reef metabolism to the bulk seawater chemistry [*Andersson and Gledhill*, 2013]. For example, higher NCP leads to higher NCC (Figure 7) and higher Ω through drawdown of CO_2 due to production, resulting in a positive correlation between NCC and Ω. The effects are more pronounced with longer residence time of the water, and lower NCC to NCP ratios as this leads to a greater range in Ω. On the reef terrace in Palmyra, the residence time is short (on the order of hours) [*Koweek et al*., 2015], and the ratio of NCC to NCP is high, further minimizing the magnitude of the feedback from benthic metabolism to bulk seawater chemistry. Therefore, the relationship observed between daily average Ω and ΣNCC in this study is likely to represent more realistic effects of CO_2 on reef NCC rates.

5. Conclusions

Here we describe the implementation of BEAMS, a rigorous system to monitor coral reef calcification dynamics using a boundary layer gradient flux approach using pH and O_2 measurements. This approach represents the first fully autonomous system to measure reef NCC in undisturbed, natural conditions on time scales of minutes. BEAMS provides a new powerful tool to observe coral reef calcification dynamics, as it is easy to deploy and operates autonomously thus providing near-continuous measurements for extended durations. Two BEAMS were successfully deployed on the western reef terrace at Palmyra Atoll in September, 2014 producing two simultaneous 2 week time series data sets of NCC and NCP rates from vastly different benthic communities. Individual deployment length was limited to 4–5 days, due to the battery capacity to operate the pumps. Use of more energy efficient pumps, lowering the supply voltage, or utilizing larger battery packs can readily extend the deployment capacity. The pH and O_2 measurements from the SeapHOx have been demonstrated to be stable for months to years [*Bresnahan et al*., 2014], making long-term deployment of BEAMS feasible. These traits make BEAMS a strong candidate to establish sustained, long-term observations for reef metabolism. Such a system would significantly improve our understanding of the environmental drivers for reef metabolism, and how they will be affected by a changing climate. As BEAMS only monitors a small region of the reef (tens of square meter), it is ideal for examining the spatial variability that may exist across different benthic communities. Coupling this system with other approaches that have a wider footprint (e.g., control volume over hundreds of square meter) would be useful to add a spatial context to our understanding.

A strong relationship between NCC and NCP was observed at both sites throughout the deployment. The ratio of NCC to NCP was significantly lower at the site dominated by an invasive noncalcifying corallimorph in contrast to the coral dominated site, further suggesting that this ratio could be a helpful tool for monitoring and managing reef health. The correlation between NCC and NCP was observed on hourly and daily time scales and was largely driven by the available light. Large variability in ΣNCC was observed, and ranged between 50 and 159 mmol $CaCO_3$ m^{-2} d^{-1}. This variability seemed to be driven by the total

available light in a given day. As this natural variability could be as large, or larger than the expected decline in NCC due to global and local anthropogenic stressors, we recommend that PAR and NCC should be simultaneously reported in future studies to enable interpretation of observed calcification rates in context of environmental variability. Such relationships were possible to observe because BEAMS provides sustained, continuous observations of NCC and NCP for multiple days.

Currently, there are only two other approaches that are capable of making fully autonomous, sustained reef metabolism observations with sub hourly resolution: control volume [*Falter et al*., 2008, 2012] and eddy covariance [*Berg et al*., 2003; *Long et al*., 2013]. However, both approaches are currently limited to NCP measurements due to a lack of an appropriate sensor (e.g., TA or calcium). NCC has been measured using a control volume approach, but discrete bottle samples for TA were used for the calculation and as a result observations were sparse [*Falter et al*., 2012]. As autonomous sensing technology for TA matures [*Crespo et al*., 2012; *Spaulding et al*., 2014], the control volume will become a powerful tool to monitor calcification dynamics on reefs. It is unlikely that a sensor for TA will be developed that is capable for an eddy covariance approach, as it requires measurements to be made at high frequencies ($>$1 Hz). Alternatively, an eddy covariance system that simultaneously measures pH and O_2 can be utilized to monitor reef NCC. Such a system has been used to monitor aerobic and anaerobic metabolism over muddy sediments [*Long et al*., 2015a], but has not yet been deployed on reefs. However, the microelectrodes utilized in eddy covariance studies are usually fragile and have a life time on the order of a few days to a week, which limits their deployment longevity and robustness for more exposed reef environments. Such traits make this approach more difficult to measure sustained reef metabolism rates for long periods of time. Development of robust, long lasting electrodes for both O_2 and pH would greatly expand the capabilities of eddy covariance for long-term reef monitoring applications. Codeployments of the gradient flux and eddy covariance approaches would be very useful to confirm that these two independent approaches using the same boundary layer theory provide the same fluxes, as has been shown for momentum [*Reidenbach et al*., 2006].

Acknowledgments

This work was funded by the National Science Foundation grants CRI-OA 1316047 and BIO OCE 1420900 and the Alfond Foundation. We thank The Nature Conservancy for logistical support on Palmyra Atoll as well as the U.S. Fish and Wildlife Service for granting research access. We would like to thank Christopher Langdon for providing the autosamplers and Eric DeCarlo for providing the sampling bottles. This research was conducted under Department of the Interior Special Use Permit #1876094 and Palmyra Atoll Research Consortium contribution PARC-#1984873. The data used in this study are available at BCO-DMO, under project BEAMS, data set Palmyra_BEAMS_2014.

References

Albright, R., C. Langdon, and K. R. N. Anthony (2013), Dynamics of seawater carbonate chemistry, production, and calcification of a coral reef flat, Central Great Barrier Reef, *Biogeosciences*, *10*, 7641–7676, doi:10.5194/bgd-10-7641-2013.

Albright, R., J. Benthuysen, N. Cantin, K. Caldeira, and K. Anthony (2015), Coral reef metabolism and carbon chemistry dynamics of a coral reef flat, *Geophys. Res. Lett.*, *42*, 3980–3988, doi:10.1002/2015GL063488.

Albright, R., et al. (2016), Reversal of ocean acidification enhances net coral reef calcification, *Nature*, *531*, 362–365, doi:10.1038/nature17155.

Al-Horani, F. A., É. Tambutté, and D. Allemand (2007), Dark calcification and the daily rhythm of calcification in the scleractinian coral, Galaxea fascicularis, *Coral Reefs*, *26*(3), 531–538, doi:10.1007/s00338-007-0250-x.

Andersson, A. J., and D. Gledhill (2013), Ocean acidification and coral reefs: Effects on breakdown, dissolution, and net ecosystem calcification, *Ann. Rev. Mar. Sci.*, *5*, 321–348, doi:10.1146/annurev-marine-121211-172241.

Anthony, K. R. N., J. A. Kleypas, and J.-P. Gattuso (2011), Coral reefs modify their seawater carbon chemistry—Implications for impacts of ocean acidification, *Global Change Biol.*, *17*(12), 3655–3666, doi:10.1111/j.1365-2486.2011.02510.x.

Atkinson, M., J. Falter, and C. Hearn (2001), Nutrient dynamics in the Biosphere 2 coral reef mesocosm: Water velocity controls NH4 and PO4 uptake, *Coral Reefs*, *20*(4), 341–346, doi:10.1007/s00338-001-0184-7.

Atkinson, M. J. (1992), Productivity of Enewetak Atoll reef flats predicted from mass transfer relationships, *Cont. Shelf Res.*, *12*(7-8), 799–807, doi:10.1016/0278-4343(92)90045-L.

Baird, M. E., and M. J. Atkinson (1997), Measurement and prediction of mass transfer to experiental coral reef communities, *Limnol. Oceanogr.*, *42*(8), 1685–1693.

Barnes, D. J. (1983), Profiling coral reef productivity and calcification using pH and oxygen electrodes, *J. Exp. Mar. Bio. Ecol.*, *66*(2), 149–161, doi:10.1016/0022-0981(83)90036-9.

Barnes, D. J., and M. J. Devereux (1984), Productivity and calcification on a coral reef: A survey using pH and oxygen electrode techniques, *J. Exp. Mar. Bio. Ecol.*, *79*, 213–231.

Bates, N. R., A. Amat, and A. J. Andersson (2010), Feedbacks and responses of coral calcification on the Bermuda reef system to seasonal changes in biological processes and ocean acidification, *Biogeosciences*, *7*(8), 2509–2530, doi:10.5194/bg-7-2509-2010.

Berg, P., H. Røy, F. Janssen, V. Meyer, B. Jørgensen, M. Huettel, and D. de Beer (2003), Oxygen uptake by aquatic sediments measured with a novel non-invasive eddy-correlation technique, *Mar. Ecol. Prog. Ser.*, *261*, 75–83, doi:10.3354/meps261075.

Boucher, G., J. Clavier, C. Hily, and J. P. Gattuso (1998), Contribution of soft-bottoms to the community metabolism (primary production and calcification) of a barrier reef flat (Moorea, French Polynesia), *J. Exp. Mar. Bio. Ecol.*, *225*(2), 269–283, doi:10.1016/S0022-0981(97)00227-X.

Bresnahan, P. J., T. R. Martz, Y. Takeshita, K. S. Johnson, and M. LaShomb (2014), Best practices for autonomous measurement of seawater pH with the Honeywell Durafet, *Methods Oceanogr.*, *9*, 44–60.

Chan, N. C. S., and S. R. Connolly (2013), Sensitivity of coral calcification to ocean acidification: a meta-analysis, *Global Change Biol.*, *19*(1), 282–290, doi:10.1111/gcb.12011.

Comeau, S., P. J. Edmunds, C. A. Lantz, and R. C. Carpenter (2014), Water flow modulates the response of coral reef communities to ocean acidification, *Sci. Rep.*, *4*, 6681, doi:10.1038/srep06681.

Crespo, G. A., M. Ghahraman Afshar, and E. Bakker (2012), Direct detection of acidity, alkalinity, and pH with membrane electrodes., *Anal. Chem.*, *84*(23), 10,165–10,169, doi:10.1021/ac302868u.

Cuet, P., et al. (2011), CNP budgets of a coral-dominated fringing reef at La Réunion, France: Coupling of oceanic phosphate and groundwater nitrate, *Coral Reefs*, *30*, suppl. 1, 45–55, doi:10.1007/s00338-011-0744-4.

Dickson, A. G. (1990), Thermodynamics of the dissociation of boric acid in synthetic seawater from 273.15 to 318.15 K, *Deep Sea Res., Part A*, *37*(5), 755–766.

Dickson, A. G., C. L. Sabine, and J. R. Christian (Eds.) (2007), *Guide to Best Practices for Ocean CO_2 Measurements*, *PICES Spec. Publ.*, *3*, 1–191.

Done, T. J. (1992), Phase shifts in coral reef communities and their ecological significance, *Hydrobiologia*, *247*(1-3), 121–132, doi:10.1007/BF00008211.

Doney, S. C., V. J. Fabry, R. A. Feely, and J. A. Kleypas (2009), Ocean acidification: The other CO_2 problem, *Ann. Rev. Mar. Sci.*, *1*(1), 169–192, doi:10.1146/annurev.marine.010908.163834.

Falter, J. L., M. J. Atkinson, and M. A. Merrifield (2004), Mass-transfer limitation of nutrient uptake by a wave-dominated reef flat community, *Limnol. Oceanogr.*, *49*(5), 1820–1831, doi:10.4319/lo.2004.49.5.1820.

Falter, J. L., R. J. Lowe, M. J. Atkinson, S. G. Monismith, and D. W. Schar (2008), Continuous measurements of net production over a shallow reef community using a modified Eulerian approach, *J. Geophys. Res.*, *113*, C07035, doi:10.1029/2007JC004663.

Falter, J. L., R. J. Lowe, M. J. Atkinson, and P. Cuet (2012), Seasonal coupling and de-coupling of net calcification rates from coral reef metabolism and carbonate chemistry at Ningaloo Reef, Western Australia, *J. Geophys. Res.*, *117*, C05003, doi:10.1029/2011JC007268.

Falter, J. L., R. J. Lowe, Z. Zhang, and M. McCulloch (2013), Physical and biological controls on the carbonate chemistry of coral reef waters: Effects of metabolism, wave forcing, sea level, and geomorphology, *PLoS One*, *8*(1), e53303, doi:10.1371/journal.pone.0053303.

Gattuso, J. P., M. Pichon, B. Delesalle, C. Canon, and M. Frankignoulle (1996), Carbon fluxes in coral reefs. I. Lagrangian measurement of community metabolism and resulting air-sea CO_2 disequilibrium, *Mar. Ecol. Prog. Ser.*, *145*, 109–121.

Gattuso, J. P., D. Allemand, and M. Frankignoulle (1999), Photosynthesis and calcification at cellular, organismal and community levels in coral reefs: A review on interactions and control by carbonate chemistry, *Am. Zool.*, *39*(1), 160–183, doi:10.1093/icb/39.1.160.

Genin, A., G. Yahel, M. A. Reidenbach, S. G. Monismith, and J. R. Koseff (2002), Intense benthic grazing on phytoplankton in coral reefs revealed using the control volume approach, *Oceanography*, *15*(2), 90–96.

Hamilton, S. L., J. E. Smith, N. N. Price, and S. A. Sandin (2014), Quantifying patterns of fish herbivory on Palmyra Atoll (USA), an uninhabited predator-dominated central Pacific coral reef, *Mar. Ecol. Prog. Ser.*, *501*, 141–155, doi:10.3354/meps10684.

Hughes, T. P., M. J. Rodrigues, D. R. Bellwood, D. Ceccarelli, O. Hoegh-Guldberg, L. McCook, N. Moltschaniwskyj, M. S. Pratchett, R. S. Steneck, and B. Willis (2007), Phase shifts, herbivory, and the resilience of coral reefs to climate change, *Curr. Biol.*, *17*(4), 360–365, doi:10.1016/j.cub.2006.12.049.

Johnson, K. S., J. P. Barry, L. J. Coletti, S. E. Fitzwater, H. W. Jannasch, and C. F. Love (2011), Nitrate and oxygen flux across the sediment-water interface observed by eddy correlation measurements on the open continental shelf, *Limnol. Oceanogr. Methods*, *9*, 543–553, doi:10.4319/lom.2011.9.543.

Kinsey, D. W. (1985), Metabolism, calcification and carbon production: 1 systems level studies, in *Proceedings of the Fifth International Coral Reef Congress*, vol. 4, pp. 505–526, Int. Assoc. of Biol. Oceanogr., Tahiti, French Polynesia.

Koweek, D., R. B. Dunbar, J. S. Rogers, G. J. Williams, N. Price, D. Mucciarone, and L. Teneva (2015), Environmental and ecological controls of coral community metabolism on Palmyra Atoll, *Coral Reefs*, *34*(1), 339–351, doi:10.1007/s00338-014-1217-3.

Langdon, C., T. Takahashi, C. Sweeney, D. Chipman, J. Goddard, F. Marubini, H. Aceves, H. Barnett, and M. J. Atkinson (2000), Effect of calcium carbonate saturation state on the calcification rate of an experimental coral reef, *Global Biogeochem. Cycles*, *14*(2), 639–654.

Long, M. H., J. E. Rheuban, P. Berg, and J. C. Zieman (2012a), A comparison and correction of light intensity loggers to photosynthetically active radiation sensors, *Limnol. Oceanogr. Methods*, *10*, 416–424, doi:10.4319/lom.2012.10.416.

Long, M. H., D. Koopmans, P. Berg, S. Rysgaard, R. N. Glud, and D. H. Søgaard (2012b), Oxygen exchange and ice melt measured at the ice-water interface by eddy correlation, *Biogeosciences*, *9*(6), 1957–1967, doi:10.5194/bg-9-1957-2012.

Long, M. H., P. Berg, D. de Beer, and J. C. Zieman (2013), In situ coral reef oxygen metabolism: An eddy correlation study, *PLoS One*, *8*(3), e58581, doi:10.1371/journal.pone.0058581.

Long, M. H., M. A. Charette, W. R. Martin, and D. C. McCorkle (2015a), Oxygen metabolism and pH in coastal ecosystems: Eddy Covariance Hydrogen ion and Oxygen Exchange System (ECHOES), *Limnol. Oceanogr. Methods*, *13*, 438–450, doi:10.1002/lom3.10038.

Long, M. H., P. Berg, K. J. McGlathery, and J. C. Zieman (2015b), Sub-tropical seagrass ecosystem metabolism measured by eddy covariance, *Mar. Ecol. Prog. Ser.*, *529*, 75–90, doi:10.3354/meps11314.

Lueker, T. J., A. G. Dickson, and C. D. Keeling (2000), Ocean pCO_2 calculated from dissolved inorganic carbon, alkalinity, and equations for K1 and K2: Validation based on laboratory measurements of CO_2 in gas and seawater at equilibrium, *Mar. Chem.*, *70*(1-3), 105–119, doi:10.1016/S0304-4203(00)00022-0.

Martz, T. R., J. G. Connery, and K. S. Johnson (2010), Testing the Honeywell Durafet for seawater pH applications, *Limnol. Oceanogr. Methods*, *8*, 172–184, doi:10.4319/lom.2010.8.172.

McCook, L. J. (1999), Macroalgae, nutrients and phase shifts on coral reefs: Scientific issues and management consequences for the Great Barrier Reef, *Coral Reefs*, *18*(4), 357–367, doi:10.1007/s003380050213.

McGillis, W. R., C. Langdon, B. Loose, K. K. Yates, and J. Corredor (2011), Productivity of a coral reef using boundary layer and enclosure methods, *Geophys. Res. Lett.*, *38*, L03611, doi:10.1029/2010GL046179.

McMahon, A., I. R. Santos, T. Cyronak, and B. D. Eyre (2013), Hysteresis between coral reef calcification and the seawater aragonite saturation state, *Geophys. Res. Lett.*, *40*, 4675–4679, doi:10.1002/grl.50802.

McManus, J. W., and J. F. Polsenberg (2004), Coral-algal phase shifts on coral reefs: Ecological and environmental aspects, *Prog. Oceanogr.*, *60*(2-4), 263–279, doi:10.1016/j.pocean.2004.02.014.

Mehrbach, C., C. H. Culberson, J. E. Hawley, and R. M. Pytkowicz (1973), Measurement of the apparent dissociation constants of carbonic acid in seawater at atmospheric pressure, *Limnol. Oceanogr.*, *18*(6), 897–907, doi:10.4319/lo.1973.18.6.0897.

Millero, F. J. (1995), Thermodynamics of the carbon dioxide system in the oceans, *Geochim. Cosmochim. Acta*, *59*(4), 661–677.

Montgomery, R. B. (1948), Vertical eddy flux of heat in the atmosphere, *J. Meteorol.*, *5*(6), 265–274, doi:10.1175/1520-0469(1948)005 < 0265:VEFOHI>2.0.CO;2.

Nyström, M., C. Folke, and F. Moberg (2000), Coral reef disturbance and resilience in a human-dominated environment, *Trends Ecol. Evol.*, *15*(10), 413–417, doi:10.1016/S0169-5347(00)01948-0.

Pandolfi, J. M., S. R. Connolly, D. J. Marshall, and A. L. Cohen (2011), Projecting coral feef futures under global warming and ocean acidification, *Science*, *333*(6041), 418–422, doi:10.1126/science.1204794.

Platt, T., C. L. Gallegos, and W. G. Harrison (1980), Photoinibition of photosynthesis in natural assemblages of marine phytoplankton, *J. Mar. Res.*, *38*, 687–701.

Reidenbach, M. A., S. G. Monismith, J. R. Koseff, G. Yahel, and A. Genin (2006), Boundary layer turbulence and flow structure over a fringing coral reef, *Limnol. Oceanogr.*, *51*(5), 1956–1968, doi:10.4319/lo.2006.51.5.1956.

Shamberger, K. E. F., R. A. Feely, C. L. Sabine, M. J. Atkinson, E. H. DeCarlo, F. T. Mackenzie, P. S. Drupp, and D. A. Butterfield (2011), Calcification and organic production on a Hawaiian coral reef, *Mar. Chem.*, *127*(1-4), 64–75, doi:10.1016/j.marchem.2011.08.003.

Shaw, E. C., B. I. McNeil, and B. Tilbrook (2012), Impacts of ocean acidification in naturally variable coral reef flat ecosystems, *J. Geophys. Res.*, *117*, C03038, doi:10.1029/2011JC007655.

Shaw, E. C., S. R. Phinn, B. Tilbrook, and A. Steven (2014), Comparability of slack water and Lagrangian flow respirometry methods for community metabolic measurements, *PLoS One*, *9*(11), e112161, doi:10.1371/journal.pone.0112161.

Shaw, E. C., S. R. Phinn, B. Tilbrook, and A. Steven (2015), Natural in situ relationships suggest coral reef calcium carbonate production will decline with ocean acidification, *Limnol. Oceanogr.*, *60*, 777–788, doi:10.1002/lno.10048.

Silverman, J., B. Lazar, L. Cao, K. Caldeira, and J. Erez (2009), Coral reefs may start dissolving when atmospheric CO_2 doubles, *Geophys. Res. Lett.*, *36*, L05606, doi:10.1029/2008GL036282.

Smith, J. E., et al. (2016), Re-evaluating the health of coral reef communities: Baselines and evidence for human impacts across the central Pacific, *Proc. R. Soc. B*, *283*, 20151985, doi:10.1098/rspb.2015.1985.

Smith, S. (1973), Carbon dioxide dynamics: A record of organic carbon production, respiration, and calcification in the Eniwetok reef flat community, *Limnol. Oceanogr.*, *18*(1), 106–120, doi:10.4319/lo.1973.18.1.0106.

Spaulding, R. S., M. D. DeGrandpre, J. C. Beck, R. D. Hart, B. Peterson, E. H. De Carlo, P. S. Drupp, and T. R. Hammar (2014), Autonomous in situ measurements of seawater alkalinity, *Environ. Sci. Technol.*, *48*(16), 9573–9581, doi:10.1021/es501615x.

Swinbank, W. C. (1951), The measurement of vertical transfer of heat and water vapor by eddies in the lower atmosphere, *J. Meteorol.*, *8*(3), 135–145, doi:10.1175/1520-0469(1951)008 < 0135:TMOVTO>2.0.CO;2.

Takeshita, Y., T. R. Martz, K. S. Johnson, and A. G. Dickson (2014), Characterization of an ion sensitive field eff ect transistor and chloride ion selective electrodes for pH measurements in seawater, *Anal. Chem.*, *86*(22), 11,189–11,195, doi:10.1021/ac502631z.

Teneva, L., R. B. Dunbar, D. A. Mucciarone, J. F. Dunckley, and J. R. Koseff (2013), High-resolution carbon budgets on a Palau back-reef modulated by interactions between hydrodynamics and reef metabolism, *Limnol. Oceanogr.*, *58*(5), 1851–1870, doi:10.4319/lo.2013.58.5.1851.

Turk, D., et al. (2015), Community metabolism in shallow coral reef and seagrass ecosystems, lower Florida Keys, *Mar. Ecol. Prog. Ser.*, *538*, 35–52, doi:10.3354/meps11385.

Uppstrom, L. R. (1974), The boron/chlorinity ratio of deep-sea water from the Pacific Ocean, *Deep Sea Res. Oceanogr. Abstr.*, *21*(2), 161–162, doi:10.1016/0011-7471(74)90074-6.

Work, T. M., G. S. Aeby, and J. E. Maragos (2008), Phase shift from a coral to a corallimorph-dominated reef associated with a shipwreck on Palmyra Atoll, *PLoS One*, *3*(8), 1–5, doi:10.1371/journal.pone.0002989.

Yates, K. K., and R. B. Halley (2003), Measuring coral reef community metabolism using new benthic chamber technology, *Coral Reefs*, *22*(3), 247–255, doi:10.1007/s00338-003-0314-5.

Yates, K. K., and R. B. Halley (2006), CO_3—Concentration and pCO_2 thresholds for calcification and dissolution on the Molokai reef flat, Hawaii, *Biogeosciences*, *3*, 357–369.

Yates, K. K., C. Dufore, N. Smiley, C. Jackson, and R. B. Halley (2007), Diurnal variation of oxygen and carbonate system parameters in Tampa Bay and Florida Bay, *Mar. Chem.*, *104*(1-2), 110–124, doi:10.1016/j.marchem.2006.12.008.

Yeakel, K. L., A. J. Andersson, N. R. Bates, T. J. Noyes, A. Collins, and R. Garley (2015), Shifts in coral reef biogeochemistry and resulting acidification linked to offshore productivity, *Proc. Natl. Acad. Sci. U. S. A.*, *112*(47), 14,512–14,517, doi:10.1073/pnas.1507021112.